Complex magnetic order from multiple Ce-sites in $Ce_3Pd_4Sn_6$

E-W Scheidt[1], A Fischer[1], O Wybranski[1], G Eickerling[1], W Scherer[1], M Baenitz[2], F Mayr[3], B Heying[4] and R Pöttgen[4]

[1] CPM, Institut für Physik, Universität Augsburg, Universitätsstraße 1, 86135 Augsburg, Germany
[2] Max-Planck-Institut für Chemische Physik fester Stoffe, Nöthnitzer Straße 40, 01187 Dresden, Germany
[3] EPV, EKM, Institut für Physik, Universität Augsburg, Universitätsstraße 1, 86135 Augsburg, Germany
[4] Institut für Anorganische und Analytische Chemie, Universität Münster, Corrensstraße 30, 48149 Münster, Germany

E-mail: Wolfgang.Scherer@physik.uni-augsburg.de and Pottgen@uni-muenster.de

Abstract

Polycrystalline $Ce_3Pd_4Sn_6$ samples were synthesized by arc-melting and subsequent annealing at 970 K. Specific heat, electrical resistivity and magnetic susceptibility measurements are performed over a wide range in temperature and provide hints for the presence of a complex magnetic ordering below 3 K arising from three crystallographically independent Ce sites. This behaviour is driven by a complex interplay between ferro-, ferri-, and antiferromagnetic correlations among the Ce atoms.

Keywords: magnetic order parameter, low temperature, magnetic susceptibility, resistivity, specific heat

(Some figures may appear in colour only in the online journal)

1. Introduction

The Ce-Pd-Sn system is characterized by the ternary stannides CePdSn [1–8], $CePd_2Sn_2$ [9, 10], the solid solution $Ce_2Pd_{2+x}Sn_{1-x}$ [11, 12], $Ce_3Pd_4Sn_6$ [13, 14], and the palladium-rich phase $Ce_8Pd_{24}Sn$ [15]. These phases have been thoroughly studied with respect to their crystal structures and magnetic properties. Equiatomic CePdSn is dimorphic. The TiNiSi-type ambient-pressure phase shows antiferromagnetic ordering at 7 K [2], while the ZrNiAl-type high-pressure modification has a lower Néel temperature of $T_{Néel} = 5$ K [8].

The magnetic behavior in the solid solution $Ce_2Pd_{2+x}Sn_{1-x}$ [11, 12] is rather complex. A sample with $x = 0.06$ first orders antiferromagnetically at 4.7 K and enters a ferromagnetic ground state at a Curie temperature of about 3.0 K. In contrast to that, for the $x = 0.21$ sample only one magnetic transition at $T_N = 3.0$ K is found. $Ce_8Pd_{24}Sn$ [15] is the stannide with the lowest tin content so far. Its structure derives from the Cu_3Au-type by an ordered filling of Pd_6 octahedral voids with the tin atoms. The Néel temperature of $Ce_8Pd_{24}Sn$ is 7 K.

$CaBe_2Ge_2$-type $CePd_2Sn_2$ [11, 12] shows Curie–Weiss behaviour over a broad temperature range. Antiferromagnetic ordering is detected as low as 0.5 K [16]. The most complex structure in the Ce-Pd-Sn system is formed by $Ce_3Pd_4Sn_6$ [13, 14]. The orthorhombic structure contains three crystallographically independent cerium atoms which fill cavities within a complex three-dimensional $[Pd_4Sn_6]$ polyanionic network. Preliminary temperature dependent magnetic susceptibility studies revealed the presence of stable Ce^{3+} characterized by an experimental effective magnetic moment of $\mu_{eff} = 2.51\ \mu_B$ / Ce-atom as derived from a Curie–Weiss fit [13]. Additionally, there was no evidence for any sort of long range order from that earlier susceptibility study above 2 K. Recent spin-polarized electronic structure calculations showed spin-polarization for all three cerium sites [14] with calculated moments of $+0.912\ \mu_B$ (Ce1), $-0.403\ \mu_B$ (Ce2), and $-0.777\ \mu_B$ (Ce3). Hence we started an experimental reinvestigation of the $Ce_3Pd_4Sn_6$ properties down to the low temperature regime ($T \geqslant 80$ mK) to survey these theoretical predictions. In this contribution we give clear evidence for the presence of a complex long range magnetic order in $Ce_3Pd_4Sn_6$

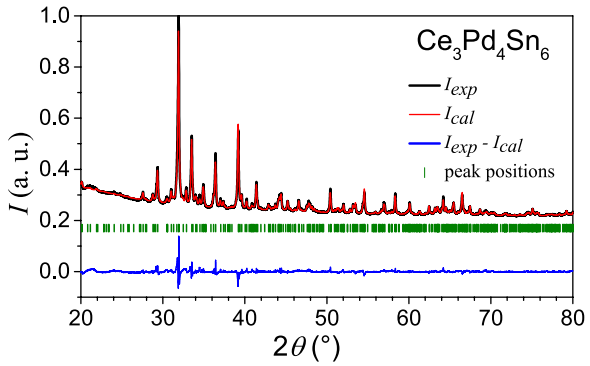

Figure 1. Comparison of the powder x-ray diffraction pattern of $Ce_3Pd_4Sn_6$, with the Rietveld-refinement (red line). The difference plot is signaled by the blue line.

involving three crystallographically inequivalent Ce-sites. Furthermore, we propose a model for a potential spin alignment pattern in the ordered state based on combined theoretical and experimental evidence.

2. Sample preparation and characterisation

Polycrystalline $Ce_3Pd_4Sn_6$ and $La_3Pd_4Sn_6$ samples were prepared by arc-melting [17] solid pieces of the pure elements (Ce: 4N, La: 3N8 (Ames MPC [18]), Pd: 3N5 (Chempur), Sn: 5 N (Heraeus)) in a purified argon atmosphere below 600 mbar. To ensure the highest homogeneity possible, the samples were turned upside-down, remelted five times, wrapped in Ta foil and finally annealed in evacuated quartz tubes for three weeks at 970 K. The weight losses of both samples after annealing were less than 0.5% of the total mass.

Polycrystalline samples of $Ce_3Pd_4Sn_6$ were measured in transmission mode on a HUBER Guinier x-ray diffractometer equipped with a Cu-$K_{\alpha 1}$-source and a HUBER G670 Guinier camera. The experimental patterns were compared to a calculated one [19], taking the atomic positions from the previous single crystal study [13]. Visual inspection of the diagrams did not reveal any traces of crystalline impurities. A Rietveld-refinement of the phase pure sample was done employing the program package JANA2006 [20], see figure 1. The refined lattice constants are $a = 1678.78(2)$ pm, $b = 459.063(3)$ pm and $c = 1557.75(6)$ pm and the refinement converged with $R = 5.43\%$.

3. Experimental techniques

The temperature dependence of the magnetic DC-susceptibility $\chi(T)$ was measured with a commercial SQUID magnetometer (MPMS7; Quantum Design) between 2 and 300 K in an external magnetic field of 1 T. Below 2 K additional magnetization measurements were performed at various magnetic fields up to 3 T using a commercial SQUID magnetometer (MPMS5), with an ^{3}He option (iQuantum Corporation) to obtain the magnetization down to 0.5 K. Both magnetometers were calibrated with a Palladium standard.

The specific heat and electrical resistivity experiments were performed using a commercial physical property measurement system (PPMS) between 2 and 300 K in magnetic fields up to 9 T. Below 2.5 K a device for the specific heat using a standard relaxation method [21] and a four-point-probe ac resistivity and ac suceptibility device were mounted in a ^{3}He/^{4}He-dilution refrigerator.

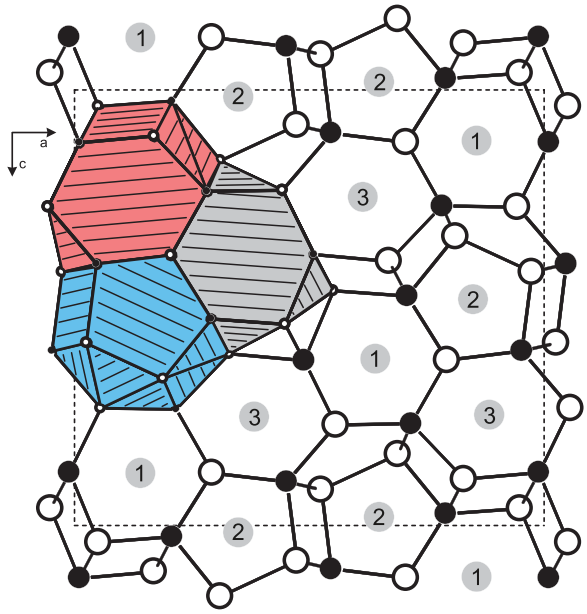

Figure 2. Projection of the $Ce_3Pd_4Sn_6$ structure onto the crystallographic *ac*-plane. Cerium, palladium, and tin atoms are drawn as medium gray, black, and open circles, respectively. The coordination around Ce1 (light grey), Ce2 (blue), and Ce3 (red) as well as the three-dimensional $[Pd_4Sn_6]$ network and atom designations for cerium are emphasized.

4. Experimental results and discussion

4.1. Crystal chemistry

$Ce_3Pd_4Sn_6$ crystallises with its own structure type, Pearson symbol oP52, space group *Pnma*. The crystal chemical details have already been described in the original contribution [13]. Herein we focus only on the relevant points concerning the cerium substructure with respect to the magnetic ordering. A projection of the $Ce_3Pd_4Sn_6$ structure onto the crystallographic *ac*-plane is presented in figure 2.

The shortest interatomic distances occur between the palladium and tin atoms. The Pd-Sn distances range from 257 to 285 pm, close to the sum of the covalent radii of 268 pm [22]. The covalently bonded $[Pd_4Sn_6]$ network leaves three types of cavities which are filled with the cerium atoms: a distorted pentagonal prism for Ce2 and distorted hexagonal prisms for Ce1 and Ce3. The rectangular faces of these prisms are more or less capped by further cerium, palladium, or tin atoms, leading to penta-capped pentagonal and hexa-capped hexagonal prisms, i.e. coordination numbers 15 and 18. The condensation pattern of the corresponding polyhedra is presented in figure 2.

The cerium substructure is shown in figure 3 as a projection onto the crystallographic *ac*-plane. The three crystallographically independent cerium sites form a slightly distorted triangular arrangement with Ce1-Ce2, Ce2-Ce3, and Ce3-Ce1

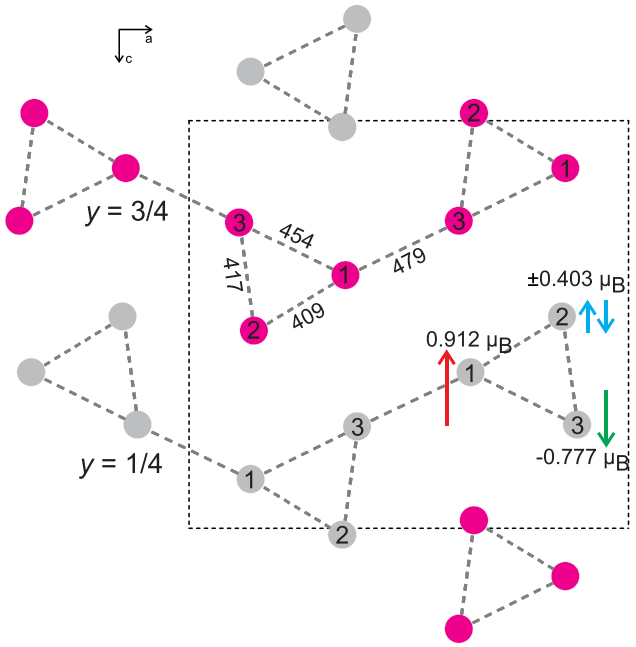

Figure 3. Projection of the cerium substructure of $Ce_3Pd_4Sn_6$ onto the crystallographic *ac*-plane. Atom designations, relevant Ce-Ce distances and a possible alignment of the magnetic moments (calculated moments from [14]) are given. For details, see text.

distances of 409, 417, and 454 pm, respectively. These Ce-Ce distances are all significantly longer than the Hill limit of 340 pm for *f* electron localization [23]. The Ce triangles are stacked along the unit cell *b*-axis with Ce-Ce distances of 459 pm, which correspond to the lattice parameter *b*. The resulting columns are connected via Ce-Ce distances of 479 pm approximately in $\pm a$ direction. Neighboring rows (shaded in magenta and grey color in figure 3) are shifted with respect to each other by half the lattice parameter *b*.

The triangular arrangement of the cerium atoms is the typical prerequisite for spin frustration, similar to the many equiatomic Ce *TX* intermetallics with ZrNiAl type structure [24]. Electronic structure calculations showed spin-polarization with significantly different moments of $+0.912\ \mu_B$ (Ce1), $-0.403\ \mu_B$ (Ce2), and $-0.777\ \mu_B$ (Ce3) [14]. These moments are drawn in the lower right-hand part of figure 3.

In this paper we suggest one possible spin alignment (labeled by arrows in figure 3), which involves a ferrimagnetic state between Ce1 and Ce3 site (also discussed by Matar *et al* [14]) and an anti-ferromagnetic coupling of the Ce2 site. In the following paragraph we underline this model with low-temperature susceptibility, specific heat and resistivity data.

4.2. Susceptibility

In figure 4(a) the temperature dependent magnetic susceptibility $\chi(T)$ of $Ce_3Pd_4Sn_6$ is presented in a linear plot between 0.5 and 15 K. The sharp peak below 2 K is the first experimental evidence for an antiferromagnetic transition at $T_{Néel} = 1.36$ K. Six years ago Samir F Matar *et al* [14] suggested a ferrimagnetic order in $Ce_3Pd_4Sn_6$, based on spin-polarized electronic structure calculations. At high temperatures the susceptibility follows a modified Curie–Weiss law:

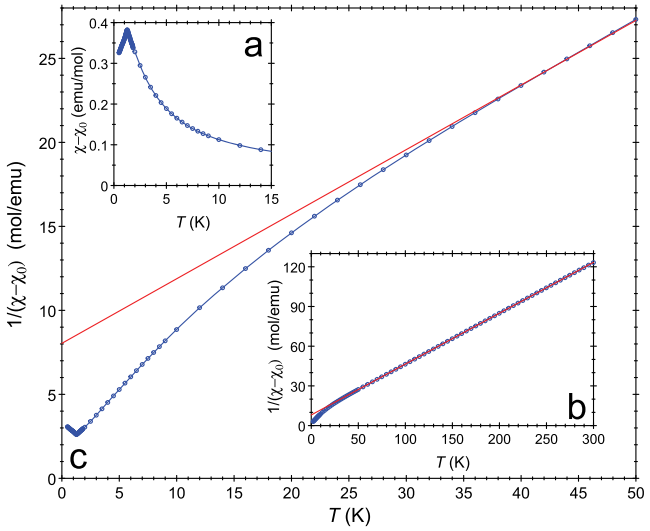

Figure 4. (a) The magnetic susceptibility $\chi - \chi_0$ versus T of $Ce_3Pd_4Sn_6$ measured in an external magnetic field of 1 T. (b) The temperature dependent reciprocal susceptibility follows a Curie–Weiss law above about 35 K. The red line is a linear fit above 40 K. (c) Enlarged plot of the reciprocal susceptibility for $T < 50$ K. The increase at very low temperatures is a clear hint for the onset of an antiferromagnetic transition. All blue lines are guides to the eye.

$\chi(T) = C/(T - \Theta_C) + \chi_0$. Here $C = 2.600(1)$ emuK mol^{-1} is the Curie constant and $\Theta_C = -20.8(1)$ K is the paramagnetic Curie temperature. The temperature independent susceptibility $\chi_0 \approx -0.176$ memu mol^{-1} is taken as a fixed value and is calculated from the sum of the Langevin diamagnetism due to the core electrons ($\approx$−0.412 memu mol^{-1}) and the Pauli paramagnetism of $\approx$0.236 memu mol^{-1}, calculated from the Sommerfeld coefficient (see section 4.3). In figure 4(b) the reciprocal susceptibility versus T reveals a linear behaviour above 35 K. From the slope of this linear fit (red line) an effective magnetic moment of $\mu_{eff} = 4.560(1)\ \mu_B$ is calculated, which is in good agreement with the theoretical value of $\mu_{eff} = 4.39\ \mu_B$ for three non-interacting Ce^{3+}-ions in the unit cell.

The enlarged plot of the reciprocal susceptibility in figure 4(c) shows a clear deviation from the linear fit to smaller values below 35 K. This observation indicates the onset of ferromagnetic fluctuations with an increasing ferromagnetic exchange interaction at decreasing temperatures. Upon cooling, the reciprocal susceptibility attains a minimum at $T = 1.36$ K, indicating an antiferromagnetic transition.

In order to obtain more insight into the complex magnetic structure and to distinguish between ferromagnetic fluctuations and an antiferromagnetic transition, low temperature dependent susceptibility measurements were performed for different magnetic fields. In figure 5(a) the temperature dependent dc-susceptibility $\chi(T)$ below 2 K is depicted for selected magnetic fields between 5 mT and 3 T. For an applied magnetic field of 5 mT a distinct antiferromagnetic transition at $T_{Néel} = 1.36$ K is observed, which is unaltered for magnetic fields up to 50 mT. Above 50 mT the antiferromagnetic transition temperature decreases with increasing magnetic fields and becomes suppressed between 1.5 and 2 T. Accompanied with the suppression of the antiferromagnetic transition, a

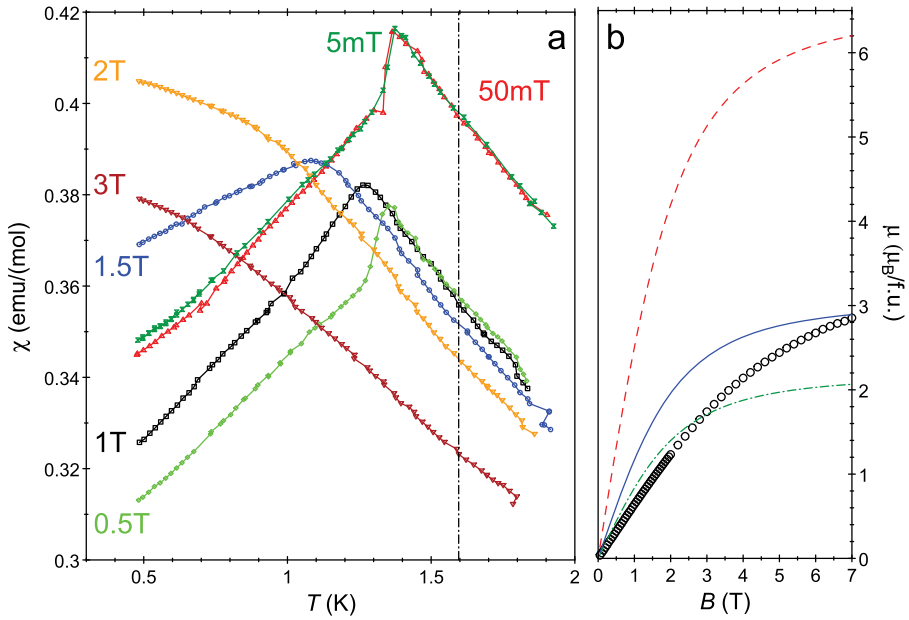

Figure 5. a) The temperature dependent susceptibility $\chi(T)$ below 2 K in various magnetic fields as labeled. The black dashed-dotted line marks the temperature of 1.6 K, where the magnetization curve shown in figure 5(b) was recorded. b) The magnetization curve $B(T)$ at 1.6 K of $Ce_3Pd_4Sn_6$ (black circles). The lines represent Brillouin functions calculated for three independent Ce-ions (red dashed line), for a single Ce^{3+}-ion only (green dashed-dotted line) and for the hypothetical model assuming 1.4 equivalents of isolated Ce^{3+}-ions per formula unit (blue solid line).

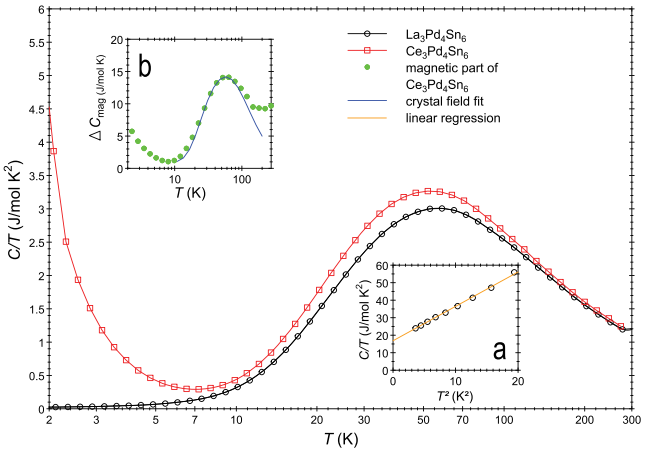

Figure 6. The temperature dependent specific heat divided by the temperature of the $Ce_3Pd_4Sn_6$ (open red squares) and $La_3Pd_4Sn_6$ (open black circles) samples in a semi-logarithmic plot between 2 and 300 K. (a) The lower insert shows the temperature dependent specific heat divided by the temperature of $La_3Pd_4Sn_6$ below 20 K, plotted versus T^2 (open black circles). The Sommerfeld coefficient is determined graphically by the interception point of the linear fit below 20 K (solid orange line) at $T = 0$ K. (b) The upper insert shows the temperature dependent magnetic contribution of the specific heat (ΔC_{mag}) for $Ce_3Pd_4Sn_6$ (full green circles). The blue solid line represents a fit of the Schottky anomaly.

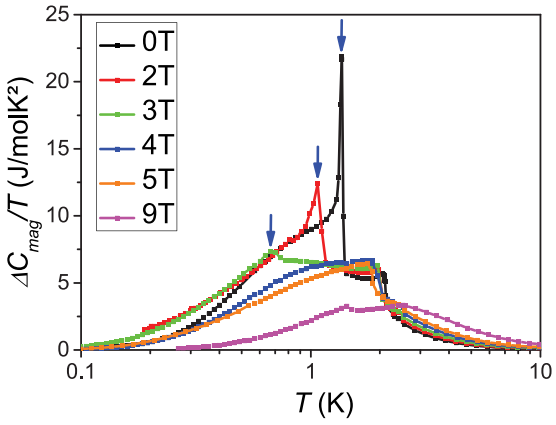

Figure 7. The temperature dependent magnetic contribution of the specific heat divided by the temperature ($\Delta C_{mag}/T$) of $Ce_3Pd_4Sn_6$ in a semi-logarithmic plot between 0.1 and 10 K for different magnetic fields up to 9 T. The blue arrows mark the magnetic transition temperatures of the lower anomaly.

possible underlying ferrimagnetic phase might dominate the temperature dependent susceptibility in magnetic fields up to 2 T. This is visible through the increase of $\chi(T)$ to lower temperatures with a negative curvature. Further increase of the magnetic field (up to 3 T) leads to a suppression of the ferrimagnetic order.

The magnetic field dependent magnetization measurement of $Ce_3Pd_4Sn_6$ at 1.6 K (shown in figure 5(b)) points to a complex magnetic order at low temperatures which may be mainly driven by the coexistence of a ferri- and an antiferromagnetic ordering. The observed magnetic moment of 2.85 μ_B at 7 T is strongly suppressed in comparison to the theoretical value of 6.21 μ_B for three independent Ce^{3+}-ions represented by the Brillouin function (red dashed line in figure 5(b)) at the same temperature and magnetic field. For a classical ferri- or ferromagnet a much steeper initial slope of the magnetization curve $\mu(B)$ is expected. Furthermore, for $Ce_3Pd_4Sn_6$, the initial slope of the experimental magnetization curve is even smaller than the slope of an idealized Brillouin function (blue solid line in figure 5(b)).

This unusual behaviour indicates a more complex magnetic ordering which may include also canted magnetism. As a first

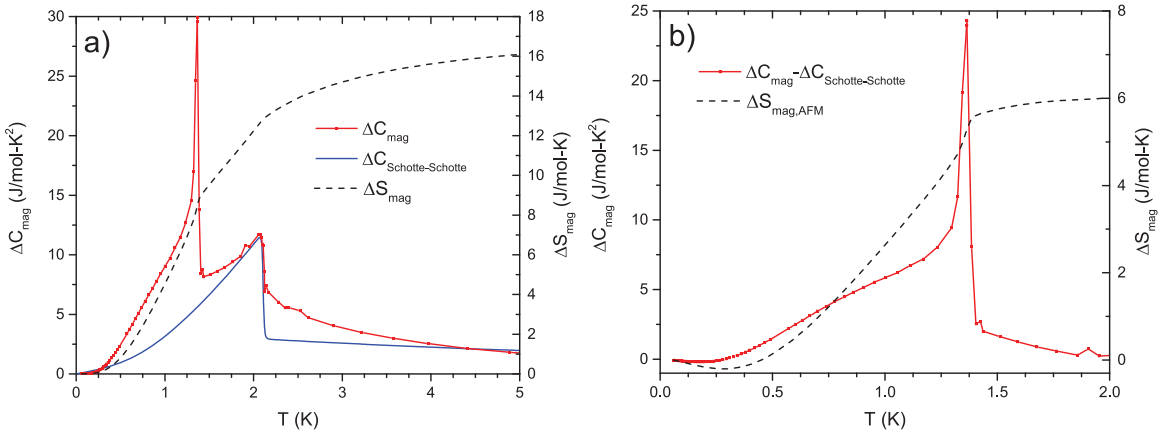

Figure 8. (a) The temperature dependent specific heat of the magnetic contribution of $Ce_3Pd_4Sn_6$ between 0.06 and 5 K (solid red squares with interconnection lines as a guide to the eye). The solid blue line is a fit using a molecular field approach according to Schotte–Schotte [25] and the dashed black line is the associated entropy contribution. (b) Difference of the temperature dependent specific heat and the Schotte–Schotte fit (solid red squares) and the dashed black line represents the corresponding temperature dependent entropy.

approximation, a simplified scenario will be discussed in the following. In figure 5(b) the green dashed-dotted line represents the Brillouin function for a single isolated Ce^{3+}-ion up to 7 T. Assuming that this Ce-ion is related to the Ce2 moment, which may be responsible for an anti-ferromagnetic order at $T_{\text{Néel}} = 1.36$ K (see section 4.1), one possible scenario is, that above $T_{\text{Néel}}$ the majority of the Ce2 moments are strongly oriented in a magnetic field of 7 T. The deviation $\Delta\mu = 0.78\ \mu_B$ between the expected magnetic moment of a single Ce^{3+}-ion ($2.07\ \mu_B$) and the experimental moment ($2.85\ \mu_B$), both at 7 T, may then be due to a canted ferrimagnetic contribution formed by the remaining Ce1 and Ce3 moments. This scenario supports the theoretical calculation [14], but implies that the ferrimagnetic transition takes place significantly above the Néel-temperature. To corroborate this complex picture, we performed low-temperature specific heat and resistivity investigations, presented in the following paragraphs.

4.3. Specific heat

In the following, we will elucidate the mechanism driving the system from a possible ferri- to an antiferromagnetic transition. First, to estimate the contribution of the conduction electrons, we determined the Sommerfeld coefficient ($\gamma = 16.8 \pm 0.3$ mJ molK^{-2}) graphically from the temperature dependent specific heat measurements of the non-magnetic La-species and the linear fit of C/T versus T^2 at $T = 0$ K is pictured in figure 6(a).

For further investigations of the three different Ce-positions in combination with the complex magnetic structure, we extracted the magnetic contribution ΔC_{mag} of the $Ce_3Pd_4Sn_6$ sample from the temperature dependent specific heat measurement by subtracting the total specific heat of the non-magnetic La species ($La_3Pd_4Sn_6$) from the corresponding $Ce_3Pd_4Sn_6$ measurement. As a result, we obtained the pure Ce based magnetic contribution, which is pictured in a semi-logarithmic plot in figure 6(b) . The broad maximum around $T = 56$ K is due to crystal field effects. The blue line is a fit to the data, taking into account a Schottky-anomaly with three Kramers doublets and a splitting energy of $\Delta_1 = 99$ K and $\Delta_2 = 250$ K.

Figure 7 shows the field dependence of the magnetic contribution of the specific heat divided by the temperature. The strong suppression of the lower anomaly with increasing magnetic field is a clear hint that the origin of this anomaly is an anti-ferromagnetic transition. For the upper transition, only a small shift with an applied magnetic field is observed, which is in line with a ferro- or ferrimagnetic transition.

The temperature dependent evolution of the magnetic entropy, $\Delta S_{\text{mag}}(T)$, is found to be 17.3 J molK^{-1} at 12 K (16.1 J molK^{-1} at 5 K, see figure 8(a)). This value is in excellent agreement with the theoretically predicted value of $\Delta S_{\text{mag}} = 3R \ln 2 = 17.28$ J molK^{-1} for three independent Ce^{3+}-ions on different Wyckoff sites. In our case each site contributes to the expected magnetic order. We used a Schotte–Schotte molecular field model [25] to describe the entropy contribution of the possible ferrimagnetic transition at around $T = 2.06$ K (Kondo temperature $T_K = 1.37$ K and exchange intercation constant $J_{\text{Sch}} = 3.75$ K), see blue line in figure 8(a). For further analysis of the lower transition, this contribution according to Schotte–Schotte has been subtracted from ΔC_{mag}, see figure 8(b). The entropy $\Delta S_{\text{mag,AFM}} = 6.0$ J molK^{-1} of the lower transition, see figure 8(b), is close to an entropy of $\Delta S_{\text{mag}} = R \ln 2 = 5.76$ J molK^{-1}, of an antiferromagnetic transition [26]. Therefore, a value of $\Delta S_{\text{mag}} = 11.3$ J molK^{-1} (up to up 12 K) remains for the upper transition which is close to $\Delta S_{\text{mag}} = 2R \ln 2 = 11.53$ J molK^{-1} and may be connected to the ferrimagnetic order formed by the magnetic moments of the Ce1 and Ce3 site as theoretically proposed by S F Matar *et al* [14]. Since there is hardly any visible signature in the temperature dependent susceptibility at $T = 2.06$ K, see figure 4(a), we assume that these magnetic moments of the Ce1 and Ce3 atoms more or less cancel each other. This would also be in line with the observations of the field and temperature dependent susceptibility data as presented in figure 5(a).

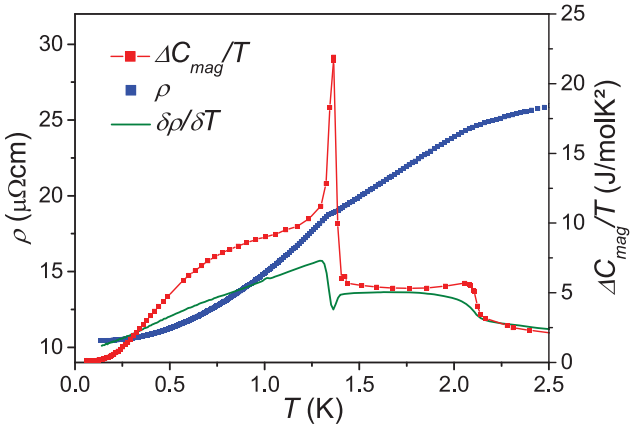

Figure 9. Comparison of the temperature dependent magnetic contribution of the specific heat divided by temperature, $\Delta C_{\mathrm{mag}}/T$, (red solid line) with the resistivity, ρ, (blue dots) and the derivative of the resistivity, $\partial\rho/\partial T$, (green solid line) of $Ce_3Pd_4Sn_6$ in a linear plot.

4.4. Resistivity

In figure 9 we compare the temperature dependent specific heat divided by temperature, $\Delta C_{\mathrm{mag}}/T$, with the resistivity behaviour, $\rho(T)$. Near the ferrimagnetic transition $\rho(T)$ exhibits a bulge. Therefore, it is not clear whether the establishment of the ferrimagnetic state occurs simultaneously, forming single ferrimagnetic pairs in each triangle between the Ce1- and Ce3-moments, or successively, first forming separately a ferromagnetic coupling between all Ce1-moments and Ce3-moments before forming a weak ferrimagnetic state. In contrast to this, at the antiferromagnetic transition a sharp kink, followed by a pronounced resistivity drop with decreasing temperatures is observed, see figure 9.

In order to obtain more detailed information from the resistivity data, we compare the $\Delta C_{\mathrm{mag}}(T)/T$ data with the derivative of the resistivity, $\partial\rho/\partial T$. In particular, the trend of the temperature dependent derivative of the resistivity is more or less similar to the temperature dependent magnetic contribution of the specific heat, at least for temperatures above $T_{\mathrm{Néel}}$. We observe significant changes of the slope $\partial\rho/\partial T$ close to the phase transition temperatures at 1.36 and 2.06 K in line with the $\Delta C_{\mathrm{mag}}(T)/T$ data.

A possible explanation for this behaviour may be, that above $T_{\mathrm{Néel}}$ the resistivity is mainly triggered by electron-magnon scattering and not by electron-impurity scattering. However, below $T_{\mathrm{Néel}}$ the derivative of the resistivity is linear, which is characteristic for pure $e^- - e^-$ scattering. Therefore a coherent electron state, as it is known from heavy fermion systems, may form a coherent lattice state at very low temperatures [27].

4.5. Discussion

From the analysis of the magnetic entropy, $\Delta S_{\mathrm{mag}}(T)$, and from specific heat studies we could clarify, that the three crystallographically independent Ce-sites control the magnetic behaviour of $Ce_3Pd_4Sn_6$ in a correlated way. Therefore we attempted to correlate the temperature dependent magnetic properties of $Ce_3Pd_4Sn_6$ with the individual Ce sites (see figure 3). Matar *et al* predicted a ferrimagnetic state established by two ferromagnetic layers of opposite spin direction [14].

Based on our entropy calculation and the temperature and magnetic field dependent susceptibility, this possible ferrimagnetic transition with very small net moment could be related to the magnetic order transition observed at $T = 2.06$ K. This transition drifts slowly to lower temperatures with increasing fields up to 5 T and shifts to 1.2 K at 9 T. In accordance with the calculations of Matar *et al* [14] we propose that the Ce1- and Ce3-sites trigger the ferrimagnetic transition, because both sites are located in a hexagonal coordination environment and therefore carry a magnetic moment of nearly the same magnitude but opposite sign. The antiferromagnetic transition at 1.36 K is unambiguously observed in the specific heat capacity, the magnetic susceptibility and electrical resistivity. This transition is drastically suppressed in an external magnetic field and vanishes at a field of approx. 3 T (see figure 7), which is typical for antiferromagnetic behaviour. In contrast to the possible ferrimagnetic transition, the antiferromagnetic transition at $T_{\mathrm{Néel}} = 1.36$ K would then most likely be controlled by the spins of the Ce2-sites which are located in a pentagonal environment (see figure 2).

5. Conclusion

Spin-polarized electronic structure calculations [14] suggest for $Ce_3Pd_4Sn_6$ the onset of a ferrimagnetic phase transition below 2 K. Based on this prediction, we have performed for the first time low temperature ($T < 2$ K) specific heat, susceptibility, and resistivity measurements. Our results support the predicted presence of a ferrimagnetic transition, which occurs at $T = 2.06$ K. In addition, the system undergoes a second transition to an antiferromagnetic ground state at $T_{\mathrm{Néel}} = 1.36$ K. Furthermore, we showed that all three crystallographically independent Ce-sites control the complex magnetic order in $Ce_3Pd_4Sn_6$ in a correlated manner. In order to clarify the complex magnetic order of $Ce_3Pd_4Sn_6$ (polarized) neutron diffraction experiments would be needed in future studies.

References

[1] Rossi D, Marazza R and Ferro R 1985 *J. Less-Common Met.* **107** 99
[2] Kasaya M, Tani T, Iga F and Kasuya T 1988 *J. Magn. Magn. Mater.* **76–7** 278
[3] Malik S K, Adroja D T, Dhar S K, Vijayaraghavan R and Padalia B D 1989 *Phys. Rev.* B **40** 2414
[4] Nakamura S, Goto T, Isikawa Y, Sakatsume S and Kasaya M 1991 *J. Phys. Soc. Jpn* **60** 2305
[5] Adroja D T and Malik S K 1992 *Phys. Rev.* B **45** 779
[6] Higashi I, Kobayashi K, Takabatake T and Kasaya M 1993 *J. Alloys Compd.* **193** 300
[7] Chevalier B, Wattiaux A and Bobet J-L 2006 *J. Phys.: Condens. Matter* **18** 300
[8] Heymann G, Riecken J F, Rayaprol S, Christian S, Pöttgen R and Huppertz H 2007 *Z. Anorg. Allg. Chem.* **633** 77
[9] Selsane M, Lebail M, Hamdaoui N, Kappler J P, Noël H, Achard J C and Godart C 1990 *Physica* B **163** 213

[10] Lidström E, Ghandour A M, Häggström L and Andersson Y 1996 *J. Alloys Compd.* **232** 95
[11] Gordon R A, Ijiri Y, Spencer C M and DiSalvo F J 1995 *J. Alloys Compd.* **224** 101
[12] Fourgeot F, Gravereau P, Chevalier B, Fournès L and Etourneau J 1996 *J. Alloys Compd.* **238** 102
[13] Niepmann D, Pöttgen R, Künnen B, Kotzyba G and Mosel B D 2000 *Chem. Mater.* **12** 533
[14] Matar S F, Rodewald U C, Heying B and Pöttgen R 2011 *Solid State Sci.* **13** 1285
[15] Jones C D W, Gordon R A, Cho B K, DiSalvo F J, Kim J S and Stewart G R 1999 *Physica* B **262** 284
[16] Kuwai T, Takagi H, Ito H, Isikawa Y, Sakurai J, Nishimura K and Paulsen C C 1998 *J. Magn. Magn. Mater.* **177–81** 399
[17] Pöttgen R, Gulden T and Simon A 1999 *GIT Labor Fachzeitschrift* **43** 133
[18] Materials Preparation Center, Ames Laboratory, US DOE Basic Energy Sciences, Ames, IA, USA, available from: www.mpc.ameslab.gov
[19] Yvon K, Jeitschko W and Parthé E 1977 *J. Appl. Crystallogr.* **10** 73
[20] Petrícek V, Dušek M and Palatinus L 2014 *Z. Kristallogr.* **229** 345
[21] Bachmann R *et al* 1972 *Rev. Sci. Instrum.* **43** 205
[22] Emsley J 1999 *The Elements* (Oxford: Oxford University Press)
[23] Hill H H 1970 *Plutonium and Other Actinides* (*Nuclear Materials Series* vol 17) ed W N Mines (New York: The Metallurgical Society of AIME) p 2–19
[24] Pöttgen R and Chevalier B 2015 *Z. Naturforsch.* **70B** 289
[25] Schotte K D and Schotte U 1975 *Phys. Lett.* A **55** 38
[26] Tari A 2012 *Specific Heat of Matter at Low Temperatures* (Singapore: Imperial Colleges Press)
[27] Stewart G R 1984 *Rev. Mod. Phys.* **56** 755